CHAPTER 3 – CORRELATING RELATIVE HUMIDITY TO DEGREE OF SATURATION INSIDE CONCRETE CROSSTIES

3.1 Abstract

Moisture levels within concrete is often assessed using relative humidity probes and sensors. However, relative humidity is a direct measurement of water vapor content and not a measurement of liquid water content. This limitation is problematic when attempting to understand the extent of liquid moisture inside concrete during freeze-thaw events. Although correlations of relative humidity to liquid water within porous media can be made, it is necessary to know the pore size distribution of the media beforehand. This distribution of pore sizes, however, may not always be known nor remain constant with respect to time inside a cement-based material. In the case of railroad high performance concrete crossties (alternatively known as ties or sleepers), the variation of pore size distributions at locations within the bulk material among thousands of concrete crossties is large. Consequently, relative humidity measurements alone cannot fully characterize the degree of saturation in concrete crossties. In this study, relative humidity sensors and electrical resistance blocks (or gypsum sensor blocks) are embedded in model concrete crossties installed in aggregate ballast. The impedance observed in these gypsum sensor blocks is directly correlated to liquid water content and is compared against the relative humidity measurements. A simple concrete adsorption isotherm model is applied in order to predict the degree of saturation from the relative humidity measurements. However, it is found that the relationship between relative humidity and degree of saturation during wetting (adsorption) and drying (desorption) in the high performance concrete is better characterized by two 3-parameter S-shaped curves.

3.2 Introduction and Background

3.2.1 Critical degree of saturation for freeze-thaw damage

Freeze-thaw damage of concrete is primarily enabled by the presence of water inside the concrete microstructure. Upon freezing, water expands by 9% of its original volume which exerts pressure onto the microstructure and results in cracking damage. Air entrainment introduces microscopically-sized air bubbles that can alleviate stresses caused by freezing water in one of

several manners: hydraulic pressure theory proposed by Powers in 1945, the diffusion and growth of capillary ice by Powers and Helmuth in 1953, the dual mechanism theory by Litvan in 1972, the osmotic pressure theory, the energy solidification theory, the ice nucleation theory, the freezing point depression, and unidirectional solidification (interface stability and stability criterion) [Carlos, 2005]. Without the presence of water in any of these cases, however, freeze-thaw damage would not occur.

The degree of saturation, *S*, in concrete is defined as the volumetric amount of liquid (V_L) and solid (V_S) water filling the open pore volume (V_P)

$$S = \frac{V_L + V_S}{V_P}. \qquad \text{Equation 3-1}$$

Alternatively, the degree of saturation can be defined as the total volumetric amount of evaporable water (V_W) at 105°C with respect to the open pore volume [Fagerlund, 1977]. This extended definition, thus, more closely adheres to the study of psychrometry where the degree of saturation is additionally defined by the volume of water vapor filling the open pore volume.

Recent research indicates that there exists a critical degree of saturation (S_{CR}) necessary for significant freeze-thaw damage to occur. Li *et al* investigated the rate of fluid ingress of different concretes with increasing amounts of entrained air content [Li *et al.*, 2012]. They found that a degree of saturation above 86-88% leads to freeze-thaw damage regardless of the amount of entrained air. The same level of damage due to freeze-thaw damage was found to occur in both poorly and properly air-entrained slabs. Several other researchers have found that there may exist a critical degree of saturation whereby no freeze-thaw damage is found to occur if the state of moisture is below the critical degree of saturation [Bentz *el al*, 2001; Litvan, 1988; Litvan and Sereda, 1980; Shimada *et al.*, 1991; Beaudoin and Cameron, 1972]. Freeze-thaw damage is often alleviated by larger measured values of entrained air which results in smaller average distances between individual entrained air voids. Thus, a freezing event in concrete with a well-dispersed spacing of air bubbles is well alleviated of high stresses. Li *et al.*, however, concluded that those specimens with poorly air-entrained voids achieved degree of saturation greater than 88% much more quickly (on the order of several days) whereas those specimens with good air-entrained voids surpassed a degree of saturation greater than 88% at a much later time (on the order of 3 to 6 years).

3.2.2 Extent of liquid moisture in high performance concrete

High performance concrete is typified by several features, one of which is incomplete hydration of the Portland cement particles by design. This incomplete hydration is accomplished by designing a low water-to-cement mass ratio and increasing the dosage of water-reducing admixtures in order to produce a workable mix that can be appropriately placed and consolidated. These low water-to-cement ratios range from 0.36 to 0.42 depending on whether saturated pores are considered [Mindess *et al.*, 2003]. As a consequence, any additional water that ingresses into the incompletely hydrated concrete matrix is purported to contribute to additional hydration which results in solid-phased hydration products (and the depletion of free liquid moisture). This phenomenon is strongly desired as the additional hydration products fills the voids in the concrete microstructure leading to a more dense and impermeable concrete matrix. Other research, in fact, has utilized saturated, porous aggregates to accomplish this purposely delayed, internal curing of the concrete microstructure [Bentz, 2009; Henkensiefken *et al.*, 2009]. High performance concrete, thus, has been postulated by some in the concrete industry to be sufficiently impermeable and resistant to the accumulation of free liquid moisture to warrant relaxed requirements on minimum air entrainment values. However, as previously discussed, it is of greater importance to understand the degree of saturation within a concrete member than it is to know its impermeability or air entrainment in order to predict the long-term performance with regards to freeze-thaw damage [Li *et al.*, 2012] and, in the specific case of railroad concrete crossties, hydrostatic pressure damage due to wheel impact loading [Zeman *et al.*, 2010].

3.2.3 Relationship between degree of saturation, absolute humidity, and relative humidity

The degree of saturation of concrete is directly assessed by measuring the volume or mass of liquid that ingresses into a known concrete volume, often through absorption testing. Water inside the concrete microstructure can exist as solid ice, liquid water, and gaseous vapor. Absolute humidity is a measurement of water content present as a gaseous vapor irrespective of the amount of water content as solid ice or liquid water. A change in the temperature or pressure affects the maximum concentration of water content in the gaseous vapor. Table 3-1 shows the vapor pressure of water, or saturation pressure, with respect to increasing temperatures. At temperatures below 0^{o}C, the vapor pressure above solid ice is dominated by sublimation. In the presence of ions in

solution, the water vapor pressure is driven downward in accordance to Raoult's Law of partial pressures, where the vapor pressure is proportional to the molar fraction of water in solution.

Absolute humidity, thus, is affected by several factors and is not often useful in assessing the degree of saturation of concrete. Instead, the absolute humidity at a given temperature can be normalized with respect to the absolute saturated humidity at that same temperature. This normalized value is called the relative humidity and is typically reported as a percent ranging from 0% to 100% when the value is measured over a flat surface of water. As such, in order to understand the degree of saturation in concrete, it is necessary to understand its relationship with the oft measured relative humidity.

Table 3-1 Change in saturation vapor pressure with respect to temperature (from Rotronic Humidity Handbook).

Temperature (°C)	Water Vapor Pressure Above Liquid (kPa)	Water Vapor Pressure Above Ice (kPa)	Ratio Ice/Liquid
-30	0.049	0.037	0.75
-25	0.081	0.064	0.78
-20	0.126	0.103	0.82
-15	0.191	0.165	0.86
-10	0.287	0.260	0.91
-5	0.422	0.402	0.95
0	0.611	0.611	1.0
10	1.23	-	-
20	2.34	-	-
30	4.24	-	-
40	7.37	-	-
50	12.33	-	-
60	19.92	-	-
70	31.18	-	-
80	47.34	-	-
90	70.11	-	-
100	101.33	-	-

3.2.4 Kelvin-LaPlace equation, modeling of pores, and hysteresis of adsorption isotherms

The Kelvin-LaPlace equation predicts the vapor pressure of a gas over the curved surface of a liquid. Its relationship is defined as

$$\frac{RT}{V_L}\ln(\frac{p}{p_s}) = 2\gamma\kappa \qquad \text{Equation 3-2}$$

where R is the universal gas constant ($^{J}/_{molK}$), T is the temperature (Kelvin), V_L is the molar volume of the liquid, p is the absolute vapor pressure and p_s is the absolute saturated vapor pressure, γ is the surface tension of the pore fluid, and κ is the curvature of the liquid surface. For a sphere with radius r_{sphere} suspended in another medium, the curvature is equal to $^{2}/_{r_{sphere}}$. In concrete, liquid moisture does not suspend itself as a collection of spheres. Instead, it adheres onto surfaces in the complex concrete microstructure. Two simple models to describe this complicated pore structure are cylinders (see Figure 3-1a) and ink-bottles (see Figure 3-1b) [Espinosa and Franke, 2006].

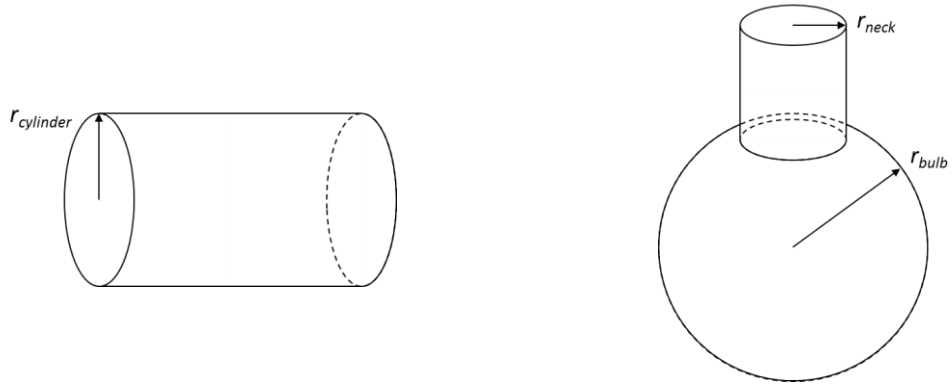

Figure 3-1 Simplification of concrete microstructure with a) cylinders (left) and b) ink-bottles (right).

For condensation of liquid onto the interior surface of a cylinder with radius $r_{cylinder}$, the curvature is equal to $-{}^{1}/_{r_{cylinder}}$. The thickness of the adsorbate, δ, can be accounted for by subtracting it from the radius as shown in Figure 3-2a. This correction leads to a revised curvature of $-{}^{1}/_{(r_{cylinder}-\delta)}$. After the cylindrical pore is fully saturated, the drying of the same cylindrical pore must be accomplished at the ends of the pore where a meniscus with radius $r_{meniscus}$ is the drying surface. The curvature of a meniscus adhered onto the interior of a cylindrical pore is $-{}^{2\cos\theta}/_{r_{meniscus}}$, where θ is the contact angle between the meniscus and the cylindrical wall. For small angles, this curvature can be approximated as $-{}^{2}/_{r_{meniscus}}$. Again, the thickness of the adsorbate can be accounted for leading to a curvature approximated as $-{}^{2}/_{(r_{meniscus}-\delta)}$ as shown in Figure 3-2b.

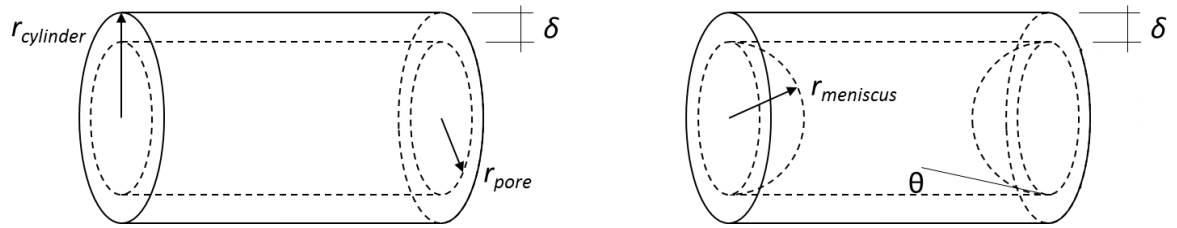

Figure 3-2 a) Wetting of the interior of a cylindrical pore with an adsorbate layer (left) and b) drying of the interior of a cylindrical pore with an adsorbate layer (right).

A similar effect is seen in an ink-bottle geometry where an adsorbate layer will grow on the inside surface of both the neck and bulb sphere of the ink-bottle until the neck becomes fully saturated. If the radius of the neck is smaller than the radius of the bulb sphere, then the neck is fully saturated while the sphere continues to grow an adsorbate layer. If the radius of the neck is larger than the radius of the bulb sphere, then the bulb sphere is fully saturated while the neck will transition to filling with a meniscus. Upon drying of the ink-bottle system, if the bulb sphere had been fully filled, then the neck will dry with a meniscus until it reaches the sphere at which a complicated drying of the sphere occurs (transitioning from a meniscus to desorption of the adsorbate layer on the bulb sphere surface). If the bulb had not been fully filled, then the sphere undergoes desorption until a meniscus forms in the neck. While a cylindrical model of pores is easier to compute, it is found that an ink-bottle model better captures the hysteretic nature of concrete adsorption curves [Espinosa and Franke, 2006].

A significant implication of the formation of menisci during the wetting and drying of pores is the resulting hysteric nature of an ideal adsorption isotherm. The wetting of a cylindrical pore has a curvature that is approximately half of the curvature of a drying meniscus. Equation 3-2 is applied to produce Figure 3-3 which is an idealized adsorption isotherm of an arbitrary distribution of pore sizes. It is evident that drying of pores results in a curve that is shifted higher than the wetting curve. This illustrates, additionally, that for a given relative humidity value, the saturation of pores can vary over a range of values as it is dependent upon the history of saturation.

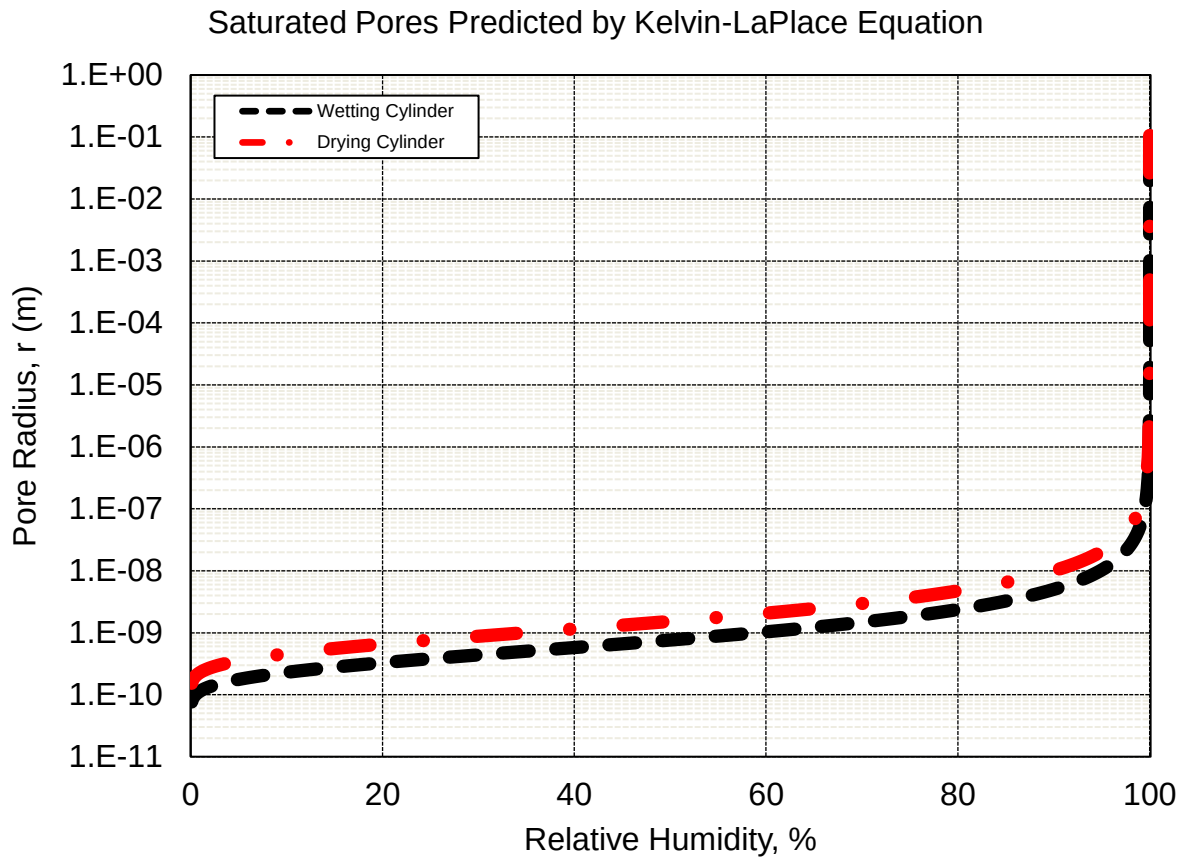

Figure 3-3 Idealized adsorption isotherm of cylindrical pores undergoing wetting and drying.

Lastly, Figure 3-3 also implies that small-radius pores become fully saturated at relative humidity values of less than 100% RH. As such, localized saturation may occur while the bulk material is not yet fully saturated. Additionally, in order for large pores (on the order of 1 μm and larger), it is necessary for there to be a constant relative humidity of 100% RH. At high relative humidity, equilibrium drives gaseous vapor to precipitate into liquid. As such, it is necessary to have both high relative humidity and a supply of adsorbate in order to continually fill very large-sized pores.

3.2.5 Typical adsorption isotherms for concrete and mortar

Isotherms can be modeled in number of different ways (Freundlich, Langmuir, BET, e.g.), yet concrete is often modeled with an empirical-fit because of the number of material challenges. Sorption isotherms for concrete are complicated by several material factors such as age, type of cement, temperature, air entrainment, water-to-cement ratio, incorporation of pozzolanic mineral

admixtures, and other material properties [Xi *et al.*, 1993; Yang, 1999; Poyet and Charles, 2009]. The effect of pores has a tremendous effect on observed relative humidity measurements. At the nano-scale within calcium-silicate-hydrate (CSH) pores, for example, the nano-pores can become fully saturated at relative humidity values of 20 %RH [Bonnaud *et al.*, 2012]. The adsorption of water within CSH swells the interlayer spacing which inherently affects the pore size distribution making this a non-linear problem. Moreover, at a larger scale of arbitrarily-sized nano-pores, the deposition of water molecules onto the pore surface can assume complicated hemispherical, conical, cylindrical, semi-elliptical, and paraboloidal menisci shapes [Dobruskin, 2008]. Additionally, concrete is a heterogeneous material wherein the pore size distribution and extent of cracking within fine aggregate, coarse aggregate, low-density hydrated cement paste (in the interfacial transition zone), and high-density hydrated cement paste are not equal.

These complications result in simplified concrete sorption curves (see Figure 3-4) where the change in mass of a concrete is shown with respect to changing relative humidity at equilibrium. The shape of the curve (additionally evident in Figure 3-3) is characterized by three phenomena: a non-linear rise near 0-10 % RH (dominated by condensation in nano- and micro-pores, linear rise between 10-80% RH (dominated by single- and multi-layer adsorption onto meso- and macro-pores), and non-linear rise at 80-100 % RH (dominated by capillary condensation in macro-pores).

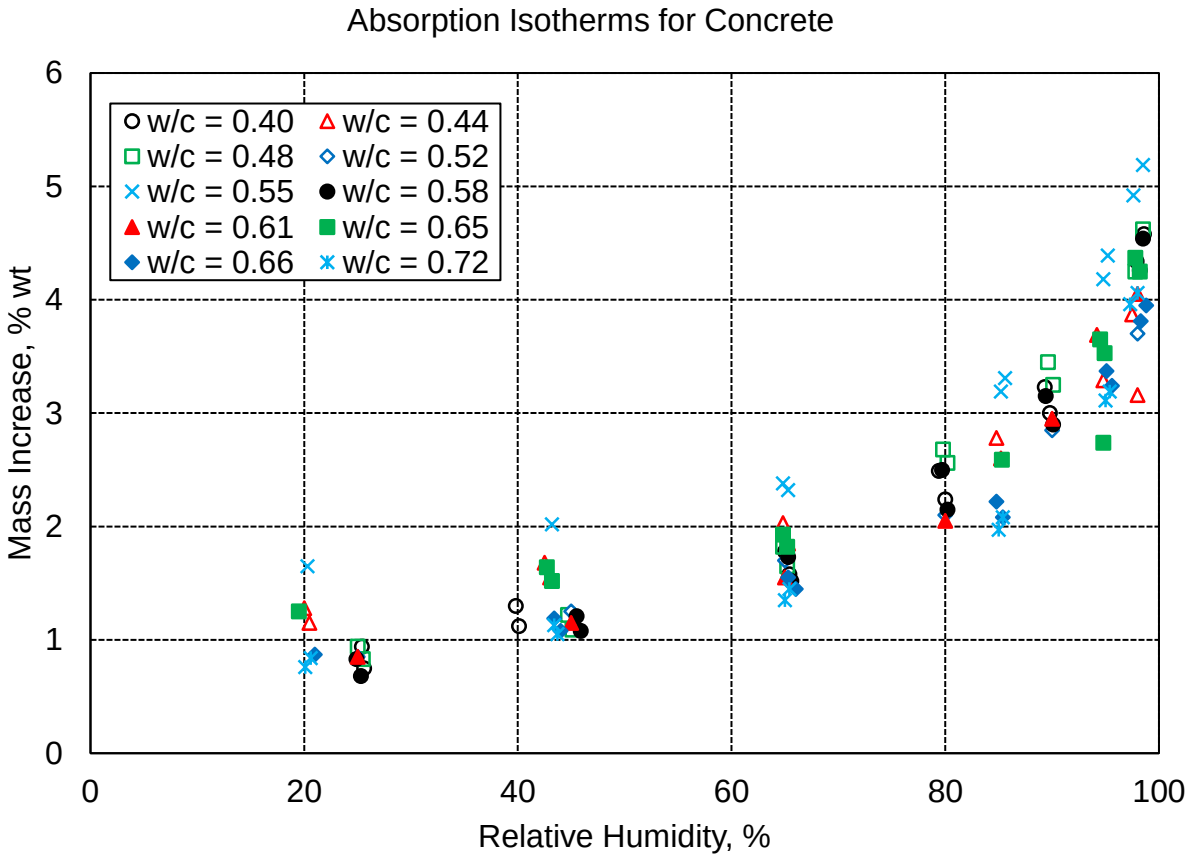

Figure 3-4 Absorption isotherms for concrete with different water-to-cement ratios (adapted from Hansen, 1986).

A simple absorption isotherm proposed by Pruckner disregards the changing material factors and assumes constant material properties as shown in the following expression

$$S = \frac{1 - ln\left|\frac{RT\ln(\frac{p}{p_s})}{\Delta\mu_{mono}}\right|}{1 - ln\left|\frac{RTln(0.999)}{\Delta\mu_{mono}}\right|} \qquad \text{Equation 3-3}$$

where $\Delta\mu_{mono}$ is the change of chemical potential at monolayer coverage [Pruckner, 2013]. Monolayer coverage of a cement-based material is primarily appropriate at low relative humidity because multi-layer coverage governs in capillary condensation. Because of this simplification, Pruckner empirically found $\Delta\mu_{mono}$ = -17.0 kJ/mol while other researchers have estimated chemical potential values of 30.7 to 42.4 kJ/mol in hardened cement paste [Adolphs and Setzer, 1996].

3.3 Significance of Research

Liquid moisture inside conventional concrete is often measured indirectly utilizing relative humidity sensors. However, relative humidity sensors alone cannot fully characterize the extent of liquid moisture within the microstructure since the relative humidity is a direct measure of vapor. Instead, it is necessary to infer a correlation between relative humidity and degree of saturation or directly measure the extent of liquid moisture. Electrical resistance blocks (or gypsum blocks) can be utilized to directly measure the degree of saturation inside concrete and be compared against complimentarily installed relative humidity sensors. Moreover, this correlation can be investigated in high performance concrete where there is incomplete hydration of the Portland cement particles. As such, a better understanding of the freeze-thaw damage potential of high performance concrete railroad crossties can be established.

3.4 Experimental Methods

3.4.1 Sensor types

Two sensor types were used in order to measure both the relative humidity and the moisture level: hygrochron sensors called iButtons (DS1923-F5) and moisture sensors called Delmhorst GB-1 Gypsum Sensor Blocks.

The hygrochron sensors feature an internally powered data acquisition system whereby two electrodes joined by a capacitive film varies in its reported dielectric constant based on changing water vapor conditions. A linear relationship between dielectric constant and relative humidity is established and modified for instances of *saturation drift* using the following expression

$$RH_{saturation\ drift\ corrected} = RH_N - \sum_{k=1}^{N} \frac{(0.0156)(\overline{RH_k})(2.54^{-0.3502k})}{1+{}^{(\overline{T_k}-25)}/_{100}} \quad \text{Equation 3-4}$$

where RH_N is the relative humidity at the end of the Nth hour when the device is exposed to high (< 70% RH) or low (< 20% RH) relative humidity, $\overline{RH_k}$ is the average relative humidity through the kth hour that that device has been exposed to high or low relative humidity, and $\overline{T_k}$ is the average temperature (in Celsius) through the kth hour the device has been continuously exposed to high or

low relative humidity. The numbers in the equation are empirical and are derived from curve-fitted data sets [Maxim Integrated, 2013].

The hygrochron sensors were fitted into iButton retainers (DS9098P) which introduced soldering points for multi-conductor shielded cabling in order to enable remote communication with each individual sensor. The sensor and retainer were fitted inside of a plastic dip coated eye bolt. A single layer of GORE-TEX fabric (a fabric that allows water vapor to pass through but not liquid water) was wrapped around each sensor in order to protect the wiring connections.

The moisture sensors are made of gypsum cast around two stainless steel electrodes and powered by an external source to induce an alternating current between the two electrodes. The advantage of an alternating current is that it prevents electrochemical effects from preferentially moving alkalis and other ions within the concrete microstructure, thusly affecting the measured results. Gypsum is a mineral ($CaSO_4 \cdot 2H_20$) that chemically interacts with Portland cement to form ettringite and thaumisite, and ground gypsum is incorporated into Portland cement during its final grinding during manufacturing [Kovler, 1998]. The gypsum sensor within hydrating and hardened concrete is susceptible to deterioration much like gypsum-rich aggregates are due to the leeching of sulfate from the sensor into the hydrated Portland cement paste that forms expansive ettringite or monosulfoaluminate (akin to alkali-silica-reaction (ASR) related expansion due to delayed ettringite attack) [Collepardi, 2003]. These ASR-related mechanisms in concrete are problematic at long time scales [Ferraris, 1995; Swamy, 2002], so they are assumed to be negligible within the 1-year time frame of this study.

The extent of liquid moisture soaked within the gypsum changes the observed impedance of the system – a high impedance denotes a dry sensor while a low impedance denotes a wet sensor. The sensors are manufactured under controlled conditions such that there is uniformity between each sensor as read by a KS-D1 Soil Moisture Meter. For this study, the moisture meter was not selected because of its inability to record and store data. Instead, an Arduino Uno R3 board was configured with an SD card microshield. The Arduino code by which the gypsum sensors collected and recorded data is located in Appendix B1.

Briefly, Pins 6 and 7 on the Arduino Uno R3 board connect to diodes (1N4148), which have a negligibly low resistance when current travels in one direction and a very high resistance in the other direction. As a consequence, an alternating current can be established by alternatively powering pins 6 and 7 off and on. After the current passes the diode connected to Pins 6 or 7, the current passes through the moisture sensor and a 1500 Ω resistor before continuing to Ground. The voltage drop is recorded with respect to Ground. A simple illustration of the moisture sensor block connection to the Arduino Uno R3 is shown in Figure 3-5 while a breakout the current travel path for Pins 6 and 7 is shown in Figure 3-6.

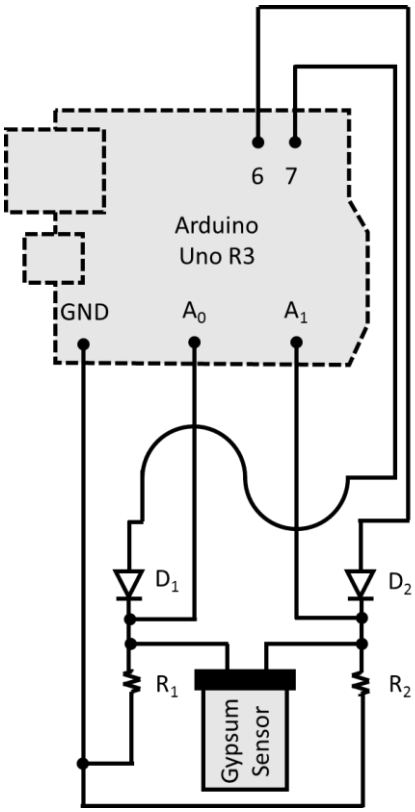

Figure 3-5 Simple illustration of one moisture sensor connected to two 1500 Ω resistors, two diodes (1N4148), and an Arduino Uno R3 microcontroller at Pins 6, 7, A0, A1, and GND.

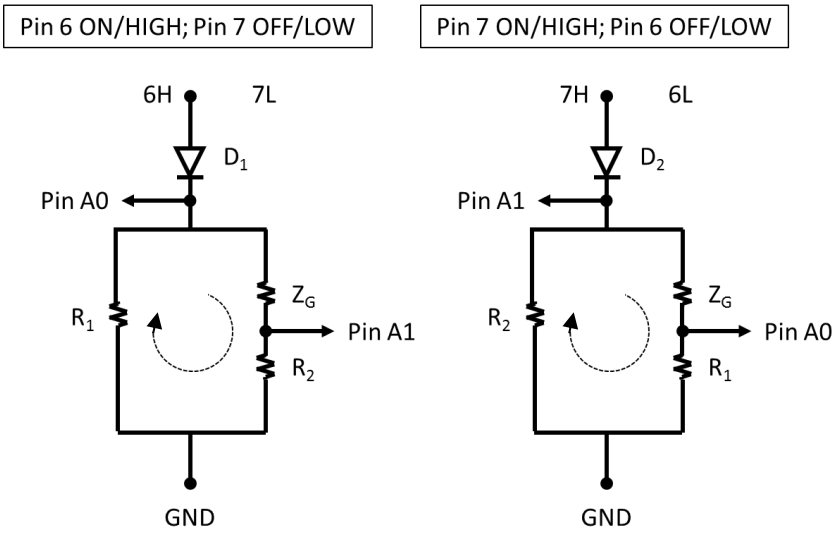

Figure 3-6 Simplified depiction of circuitry when a) Pin 6 voltage is HIGH (left) and b) when Pin 7 voltage is HIGH (right).

In the instance when Pin 6 is set to a HIGH voltage and Pin 7 is set to a LOW voltage (see Figure 3-6a), analog Pin A1 measures the voltage drop with respect to GND across R_2 on the right-hand-side of the circuit branch. The current across the right-hand-side, I_{RHS}, of the circuit can be expressed as

$$I_{RHS} = {\Delta V_{R2}}/{R_2} \qquad \text{Equation 3-5}$$

where ΔV_{R2} is the measured voltage drop with respect to GND across R_2. Analog Pin A0 measures the voltage drop with respect to GND across the two branches of the circuit (left-hand-side and right-hand-side). Seemingly, Pin A0 measures a set of known and unknown resistors in parallel and series. However, Kirchoff's second law states that closed loops within a circuit must have its voltage drops and gains equate to zero. As such

$$\sum \Delta V_{\circlearrowleft} = \Delta V_{ZG} + \Delta V_{R2} - \Delta V_{R1} = 0 \qquad \text{Equation 3-6}$$

where ΔV_{R1} is the measured voltage drop with respect to GND across R_1 and where ΔV_{ZG} is the measured voltage drop with respect to GND across Z_G. As such

$$\Delta V_{ZG} + \Delta V_{R2} = I_{RHS}(Z_g + R_2) = \Delta V_{R1} = I_{LHS}R_1. \qquad \text{Equation 3-7}$$

Although the current along the left-hand-side and right-hand-side of the branches do not equal, by Kirchoff's first law, the current along the right-hand-side across both resistors must equal. As such, Equation 3-5 and 3-7 can be equated

$$I_{RHS} = {\Delta V_{R2}}/{R_2} = {(\Delta V_{ZG} + \Delta V_{R2})}/{(Z_g + R_2)}. \quad \text{Equation 3-8}$$

Following several simplifying mathematical steps, the unknown impedance of the moisture sensor, Z_G, can be solved as

$$Z_g = {R_2}/{\Delta V_{R2}}\,[(\Delta V_{ZG} + \Delta V_{R2}) - \Delta V_{R2}], \text{ or}$$

$$Z_g = {R_2}/{A1}\,[A0 - A1] \quad \text{Equation 3-9}$$

where *A0* and *A1* are the voltage values measured by analog Pins A0 and A1, respectively. An analogous derivation can be made in the instance when Pin 7 is set to HIGH and Pin 6 is set to LOW (see Figure 3-6b). A single Arduino Uno R3 microcontroller board has six analog input pins, meaning that three moisture sensor blocks can be configured if dual readings are made (that is to say, setting Pins 6 and 7 HIGH on a single sensor). In order to increase the number of moisture sensors that can be monitored at a single installation site, a single reading can be taken (e.g. when Pin 7 is set to HIGH) while still exciting both pins in order to achieve an alternating current. In doing so, electrochemical processes can be prevented while a gain in the number of moisture sensors is achieved. Figure 3-7 shows the complete circuitry deployed where Pin 7 is set to HIGH during data recording.

The hardware is powered by a 10000 mAh external battery power pack and is housed inside a metal junction box in order to protect the circuitry from the natural elements (see Figure 3-8).

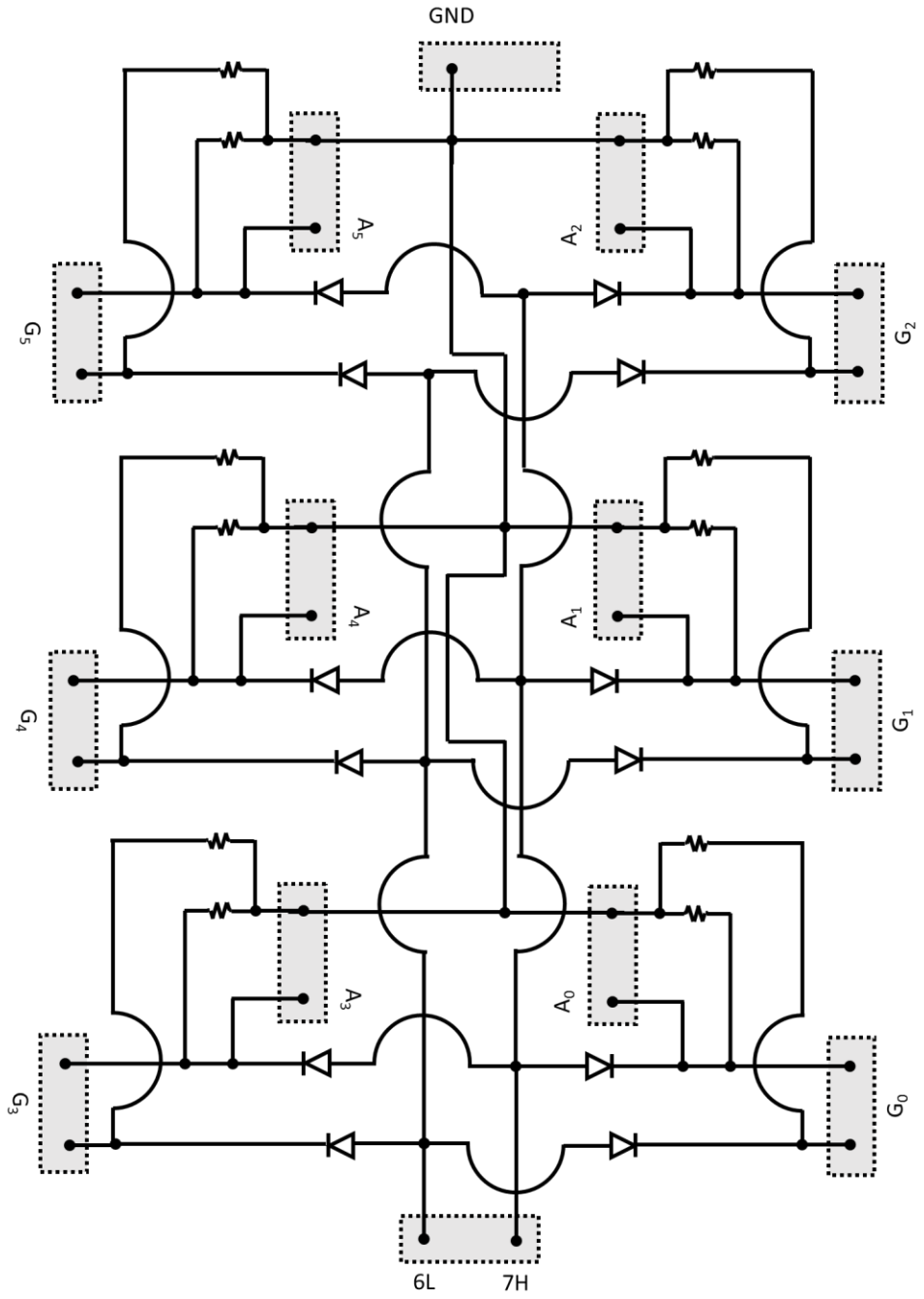

Figure 3-7 Complete circuitry scheme where six moisture sensor blocks (G0-G5) are measured for their change in impedance when Pin 7 on an Arduino Uno R3 microcontroller board is set to HIGH. In order to prevent electrochemical deterioration processes, Pin 6 is also set to HIGH in an alternative manner in order to mimic an alternating current.

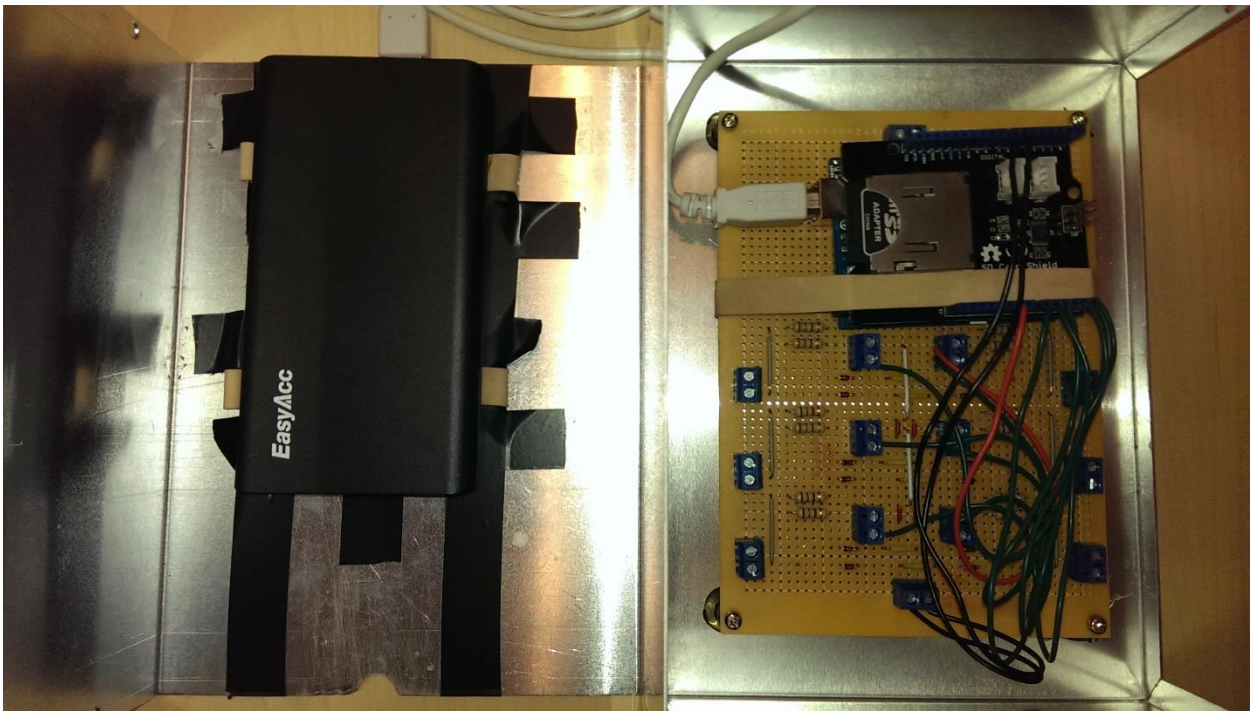

Figure 3-8 Image of hardware where an SD shield is connected above an Arduino Uno R3 microcontroller board. The Arduino and shield are securely fastened with a rubber band onto a circuit board that is wired in accordance in Figure 3-7. A 10000 mAh external battery back provides an approximate seven day charge for the hardware to operate independently. The entire setup is encased in a metal junction box.

3.4.2 Calibration of moisture sensor

The moisture sensor block directly reports the impedance of the sensor. In order to calibrate the sensor reading to a degree of saturation, the mass of the sensor was measured with respect to the impedance. This calibration was accomplished by suspending the sensor at one end of an instrumented cantilever beam of known stiffness. The change in the bending moment before and after immersing the sensor in water is collected across several days. Repeated instances of wetting and drying of the moisture sensor block was performed in order to enhance confidence in the calibration.

3.4.3 Preparation of installation method

Both the hygrochron sensors and the moisture sensors were installed onto a steel angle bracket with unthreaded holes spaced one inch apart (see Figure 3-9). The hygrochron sensors were installed at depths of 0.5, 2.5, 5.5, and 8.5 inches from the top surface of the model concrete

crosstie. The moisture sensors were installed at depths of 0.5, 2.5, and 8.5 inches from the same top surface (see Figure 3-10).

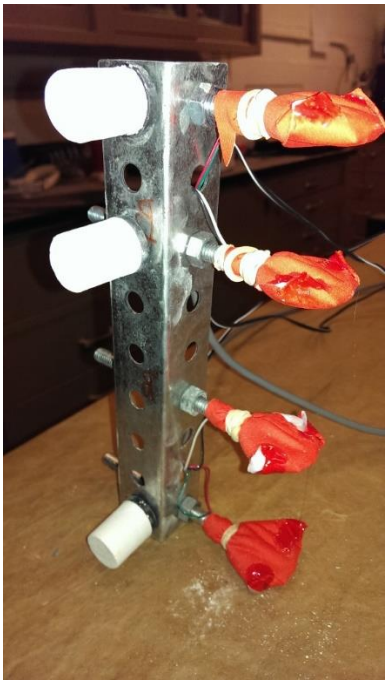

Figure 3-9 Construction of hygrochron sensors seated inside an iButton retainer installed in a plastic dip coated eye bolt and sealed with a single layer of GORE-TEX fabric. A rubber band securely holds the fabric in place. Moisture sensor blocks are additionally installed along the orthogonal face of the angled steel bracket.

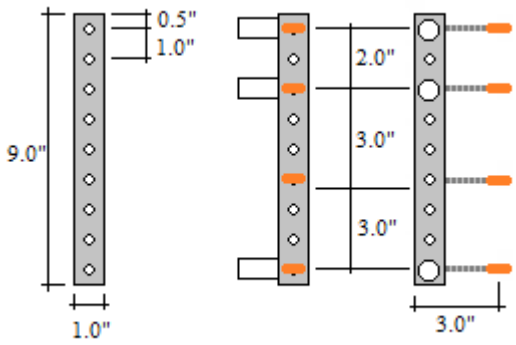

Figure 3-10 Depiction of nine inch tall bracket (left) with half-inch clearance at top and bottom. Hygrochron sensors (orange) and moisture sensors (white) are affixed at depths as depicted (right).

3.4.4 Instrumentation of model concrete crossties and installation in model ballast

The steel angle brackets were installed into two molds measuring 9-inch by 9-inch by 16-inches. These dimensions are comparable to the cross-section dimensions of a typical concrete

crosstie. One of the molds was fashioned with steel fastening anchors such that a polyurethane pad and rail section could be affixed at a later time (see Figure 3-11a). The instrumented bracket was positioned such that the hygrochron sensor and moisture sensor were geometrically centered about the rail seat area and additionally symmetric to each other across the horizontal centerline of the mold (see Figure 3-11b). The concrete mixture design is shown in Table 3-2, and is intended to be comparable to typical high performance concrete crossties with a water-to-cement mass ratio of 0.30.

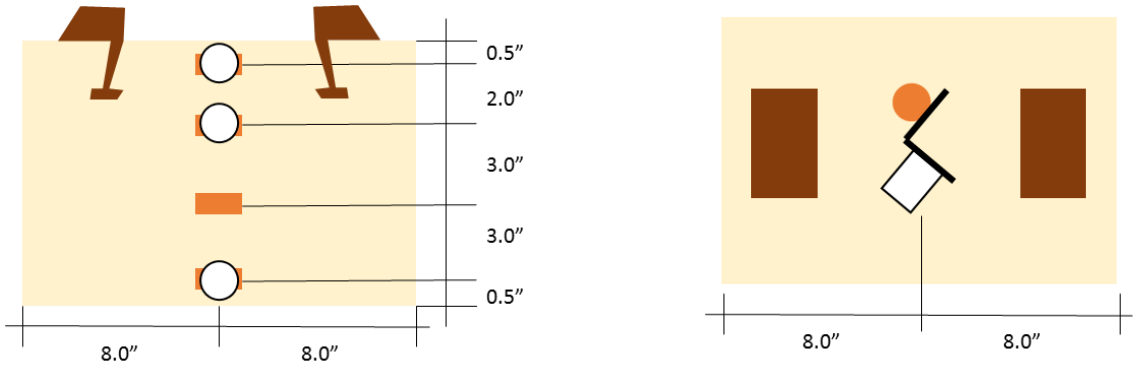

Figure 3-11 Diagram of instrumented model crosstie with both hygrothermal sensors and moisture sensors installed at various depths (left). The plan view (right) of the model crosstie depicts the approximate positioning of the sensors such that they are geometrically centered within the rail seat area and symmetric to each other across the horizontal centerline.

Table 3-2 Nominal concrete mix design of model crossties.

Material Type	**Pounds Per Cubic Yard**	**Kilograms Per Cubic Meter**
Type I Portland Cement	718	426
#7 Aggregate	2085	1236
Sand	1257	746
Water	216	128
High Range Water Reducer	12 fl. oz / 100 lb. cementitious (782 mL per 100 kg cementitious)	

The model crossties were demolded (see Figure 3-12) and cured in an environmentally controlled room at 23°C and 50% RH. Thereafter, the model crossties were installed in model ballast in Rantoul, IL. The model ballast is a 1-1.5 inch top-size yard ballast that conforms to Union Pacific Railroad (UPRR) Class-2 Ballast Specifications. The model ballast sits atop an angled asphalt lot, which facilitates rainfall runoff and prevents stagnant water from building within the ballast. The model crossties were installed at one end of the ballast where the distance separating the underside of the model crossties and the surface of the asphalt lot is 5 to 6 inches. The model

crosstie was positioned such that its surface was flush with the model ballast. Additionally, a polyurethane pad and steel rail section was added to the model crosstie with embedded anchors (see Figure 3-13a).

Figure 3-12 De-molded model concrete crossties with PVC access plug where multi-conductor shielded cables are encase.

Figure 3-13 Model crossties installed in model ballast in Rantoul, IL. A polyurethane pad and steel rail section is added to the model crosstie with embedded anchors.

3.5 Results, Discussion, and Empirical Modeling

3.5.1 Relative humidity results over observation period

Although relative humidity of ambient conditions fluctuates daily, the internal relative humidity of concrete members fluctuates in a more seasonal manner. Figure 3-14 shows a model concrete crosstie installed from an environmentally controlled environment to an aggregate ballast

located in Rantoul, IL. Relative humidity sensors near the surface of the model concrete crosstie show a gradual increase in relative humidity while relative humidity sensors inside the bulk material (at 2.5 an and 5.5 inches from the top surface) are fairly unaffected by the installation into an aggregate ballast.

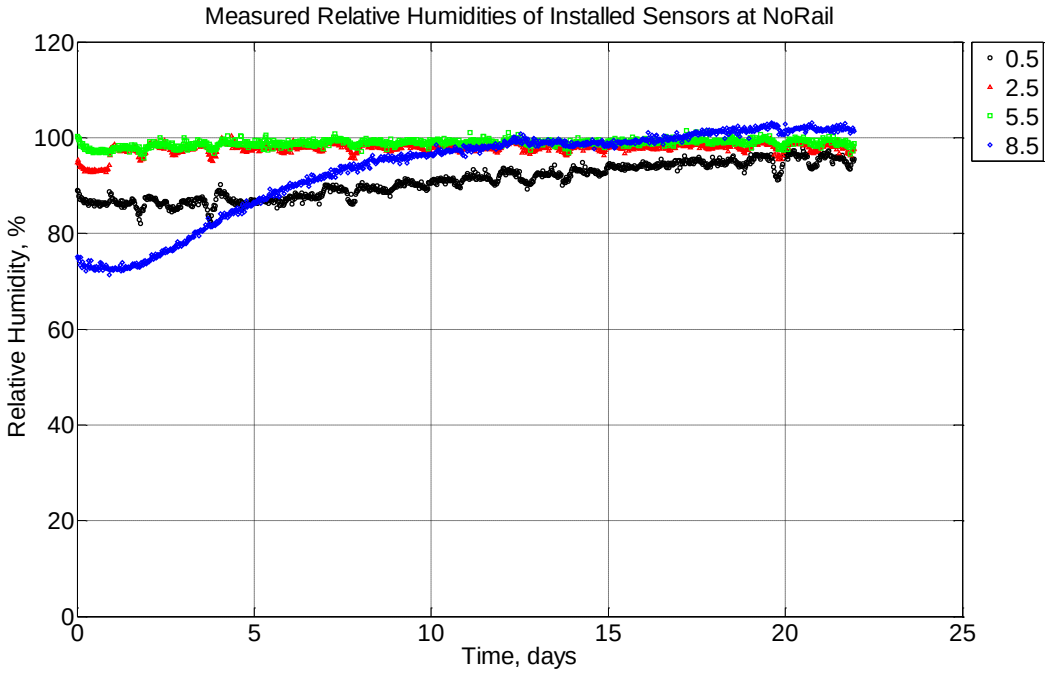

Figure 3-14 Measured relative humidity at depths of 0.5 inches (12.7 mm), 2.5 inches (63.5 mm), 5.5 inches (139.7 mm), and 8.5 inches (215.9 mm) from the surface of a model concrete crosstie (labeled NoRail) without a polyurethane pad nor rail installed in ballast in Rantoul, IL, between November 29, 2014, through December 21, 2014.

3.5.2 Predicting degree of saturation based on measured impedance

The moisture sensor blocks and Arduino algorithm (see Equation 3-9 and Appendix B1) directly report the impedance, Z_G, of each sensor. However, the impedance measurement can be calibrated against varying degrees of moisture. Figure 3-16 shows the graphical result of two uniformly manufactured moisture sensors undergoing 5 instances of drying and soaking cycles. The curves across the 5 instances overlay each other, so a power-law function is fitted to a representative section of the data to with a high fit of R^2 of 0.98. As such, the independently measured impedance value, Z_G, and estimated degree of saturation, S, can be related by the following power-law expression

$$Z_g = 817.14S^{-1.284}. \qquad \text{Equation 3-10}$$

This expression can be solved for in terms of S to yield

$$S = \left({}^{Z_g}/_{817.14}\right)^{({}^{1}/_{-1.284})}. \qquad \text{Equation 3-11}$$

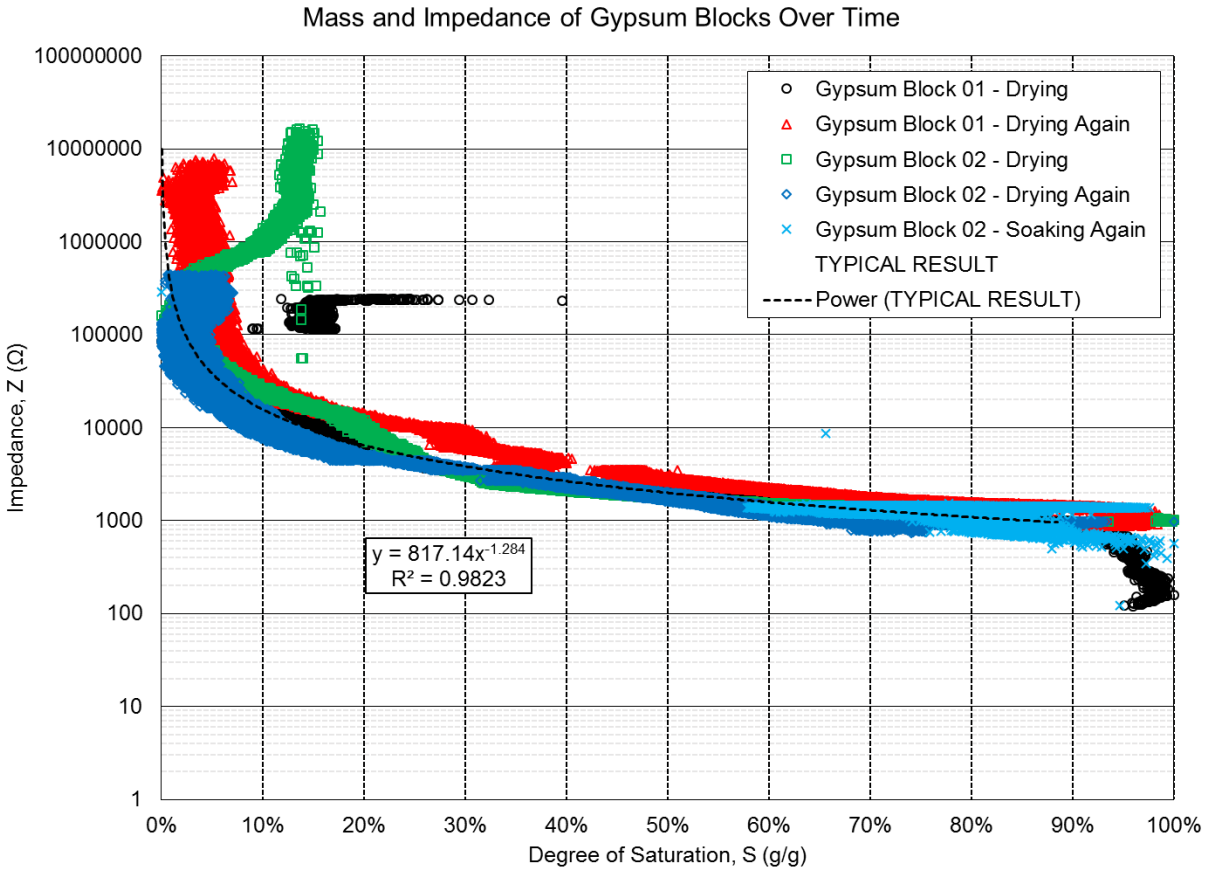

Figure 3-15 Change of mass and impedance of two moisture sensors undergoing drying and soaking. The change in mass is normalized to the soaked mass in order to create a degree of saturation.

3.5.3 Degree of saturation results over observation period

The degree of saturation inside the model concrete crossties is estimated based on Equation 3-11 and the measured impedance value of the moisture sensor block. The result of three moisture sensors soon after installation in aggregate ballast in shown in Figure 3-16. It is evident that the two sensors near the surface (0.5 and 8.5 inches) are nearly at 0 % degree of saturation while the

interior sensor (2.5 inches) maintains a high degree of saturation at 100%. However, soon after installation into the aggregate ballast, the moisture sensors indicate an increase in liquid moisture. In particular, the sensor at the top surface (0.5) gradually increases to a high degree of saturation by day 12. The sensor at 8.5 inches from the top surface shows an upward trend before stabilizing at a relatively low degree of saturation. The sensor at 2.5 inches shows very little change until several weeks later (February 10, 2015) (see Figure B2-13 in Appendix B)when its values are comparable to the other sensors embedded at 0.5 and 8.5 inches suggesting that the internal moisture conditions in this young-age concrete (mixed 40 days prior to the data presented in Figure 3-16) is high.

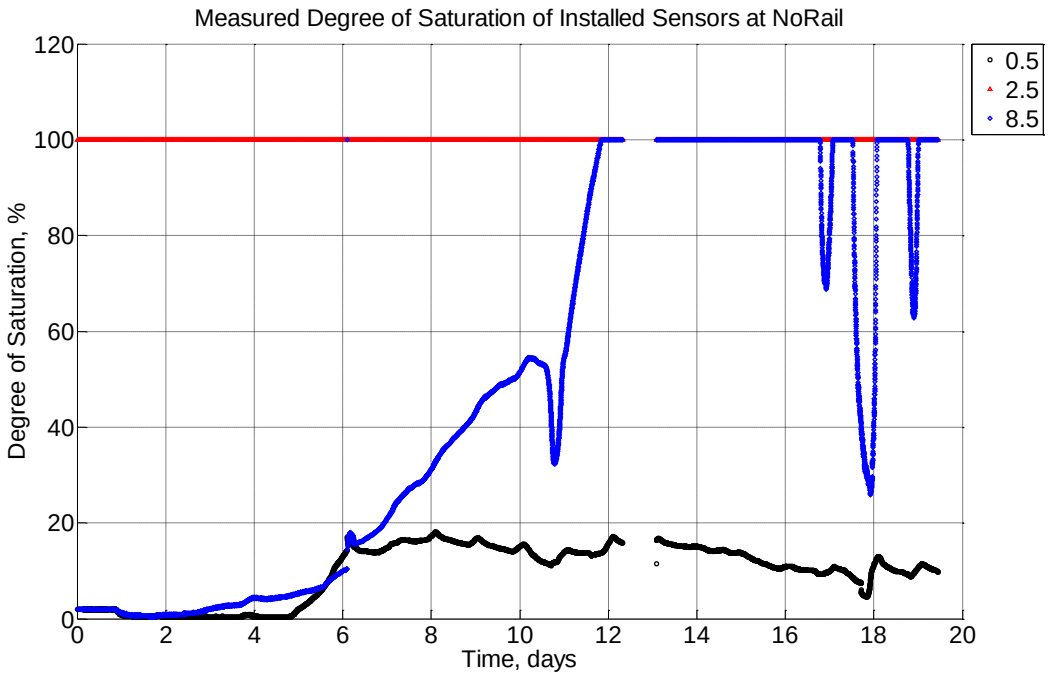

Figure 3-16 Measured degree of saturation at depths of 0.5 inches (12.7 mm), 2.5 inches (63.5 mm), and 8.5 inches (215.9 mm) from the surface of a model concrete crosstie (labeled NoRail) without a polyurethane pad nor rail installed in model ballast in Rantoul, IL, between December 1, 2014, through December 21, 2014.

Two sensors (at 0.5 and 8.5 inches from the top surface) exhibit unusual troughs that are sudden and coincidental on days 10, 17, 18, and 19. On these days, it is evident that ambient temperatures fell to below 0^{o}C (see Figure A10-5). It is likely that portions of the water inside the concrete crosstie and within the moisture sensor block transformed from liquid water to solid ice. As such, the impedance between the two electrodes would be altered because of the change in

conductivity of liquid water and ice. These instances of depressed degree of saturation are artificial and the analysis can be improved by calibrating the moisture sensor at multiple temperature ranges. Moreover, the stagnation of the gypsum sensor block at S = 100% at 2.5 inches draws the question whether the gypsum sensor is preferentially retaining water due to a finer pore size distribution. The approximate range of moisture diffusivity for gypsum is 5.4×10^{-6} to 4.8×10^{-3} m^2/hr from dry to saturated [Tesárek *et al.*, 2004] as compared to the diffusivity of concrete from 6.8×10^{-7} m^2/hr [Qin and Hiller, 2014] to 2.02×10^{-6} m^2/hr [Kang *et al.*, 2012], meaning that moisture diffusion through concrete should be occurring more slowly in relation to the gypsum sensor block. As a consequence, the measured values in the gypsum should not represent a state in which the moisture level is preferentially higher in the gypsum sensor than the concrete bulk material.

3.5.4 Comparing degree of saturation with relative humidity measurements

Measured relative humidity (such as in Figure 3-14) can be compared against measured degree of saturation (such as in Figure 3-16) to produce a correlation of data (see Figure 3-17). This depiction of the data is in keeping with how sorption isotherms are displayed. However, several key differences are noted:

- The temperature represented within Figure 3-17 is not constant, therefore there is no isothermal constraint on the result.
- Equilibrium of relative humidity and equilibrium of degree of saturation are not reliably attained due to extreme fluctuations due to ambient conditions.
- The distribution of pore sizes is assumed to be constant. This assumption is irrespective of the nature of high performance concrete which has unreacted Portland cement particles leading to densification of pore structure when exposed to additional liquid water.

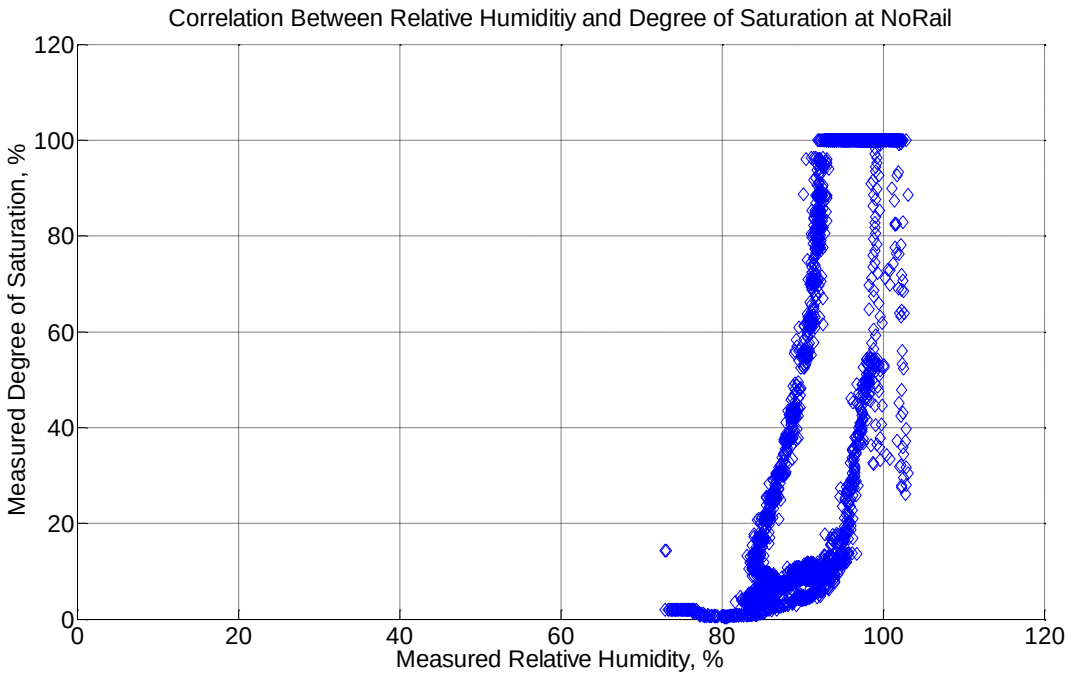

Figure 3-17 Correlation between measured relative humidity and degree of saturation at depth of 8.5 inches (215.9 mm) from the top surface of a model concrete crosstie (labeled NoRail) without a polyurethane pad nor rail installed in model ballast in Rantoul, IL. The data represents two periods from December 1, 2014, though December 21, 2014, and June 20, 2015, through September 11, 2015.

3.5.5 Comparing degree of saturation with predictive adsorption isotherm

Any number of adsorption isotherms can be compared against the result in Figure 3-17. Figure 3-18 shows one such adsorption isotherm by Pruckner [Pruckner, 2013]. It is readily apparent that the predictive adsorption isotherm does not represent the observed data set nor would many other isotherms. This is principally due to the experimentally measured degree of saturation reducing to 0% at instances when the relative humidity is greater than 80%. Such a behavior is mostly likely attributable to a low water-to-cement ratio leading to ongoing hydration of unreacted cement particles.

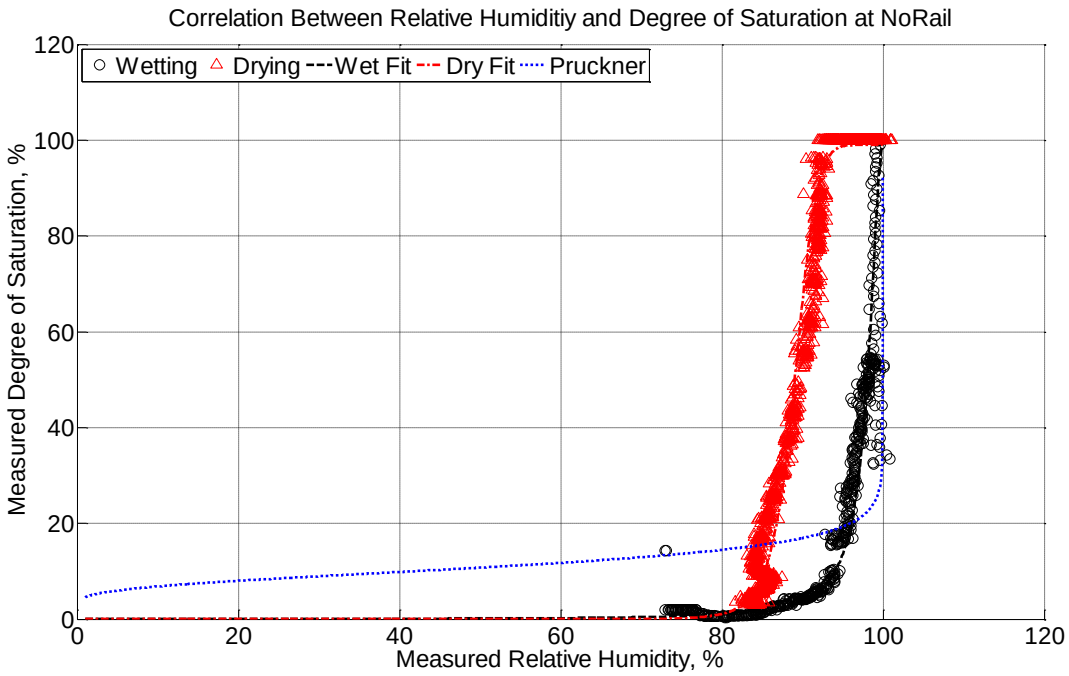

Figure 3-18 Correlation between measured relative humidity and degree of saturation at depth of 8.5 inches (215.9 mm) from the top surface of a model concrete crosstie (labeled NoRail) without a polyurethane pad nor rail installed in model ballast in Rantoul, IL. The black circles represent a wetting cycle that occurs from December 6, 2014, though December 13, 2014, while the red triangles represent a drying cycle that occurs from June 20, 2015, through September 11, 2015.

The correlation between degree of saturation and relative humidity in Figure 3-18 is also separated into two distinct phases: wetting and drying. When done so, it is apparent that there is hysteresis between the two curves. As such, the notion of a complex pore structure (cylindrical, ink-bottle, e.g.) is evident. Moreover, it is important to note that the wetting curve is accomplished in less than one week whereas the drying curve is accomplished in approximately three months. The drying curve was achieved by placing a breathable water-resistant canvas tarp over the model concrete crosstie. This is indicative of typically faster absorption rates of concrete versus slower desorption rates.

An implication of freeze-thaw damage is that there can persist a long period of highly saturated concrete while a precipitation event would have occurred months earlier. Additionally, the hysteretic nature of the correlation between degree of saturation and relative humidity indicates that a single measurement of relative humidity (93% RH, e.g.) can be interpreted in two vastly different manners: a degree of saturation as low as 15% and as high as 100%. As such, a single

measurement of relative humidity must be understood in a contextual manner as it cannot be understood as a singular event.

In the case where incomplete hydration of the Portland cement particles is evident (leading to a result where degree of saturation values fall to 0% while relative humidity remains high at values of 80% RH), it is possible to empirically fit an expression to predictively estimate the degree of saturation based on a measured relative humidity value. It is observed that a 3-parameter S-shaped curve can adequately represent the wetting and drying curves. As such, the degree of saturation, *S*, can be estimated as

$$S = S_o\left(\beta_o \frac{1-\beta_o}{1+\left(1-RH/1-RH_b\right)^m}\right) \qquad \text{Equation 3-12}$$

where S_o is 100% RH, β_o is a fit parameter affecting the y-axis range, RH_b is a fit parameter affecting the x-axis range, and m is a fit parameter affecting the curvature of the graph. The values used for both the wetting and drying curves are shown in Table 3-3 and the fit between the model and experimental data are shown in linear scale in Figure 3-18 and log scale in Figure 3-19. These wetting and fitting curves represent envelopes of degree of saturation based on measured relative humidity values. In the event that relative humidity does not follow this envelope, then an intermediary expression predictively governs the relationship between degree of saturation and relative humidity.

Table 3-3 Fit parameters used for 3-parameter S-shaped curves for wetting and drying curves.

Parameter	**Wetting Curve**	**Drying Curve**
β_o	0.01	0.01
RH_b	98% RH	89% RH
m	2	7.5

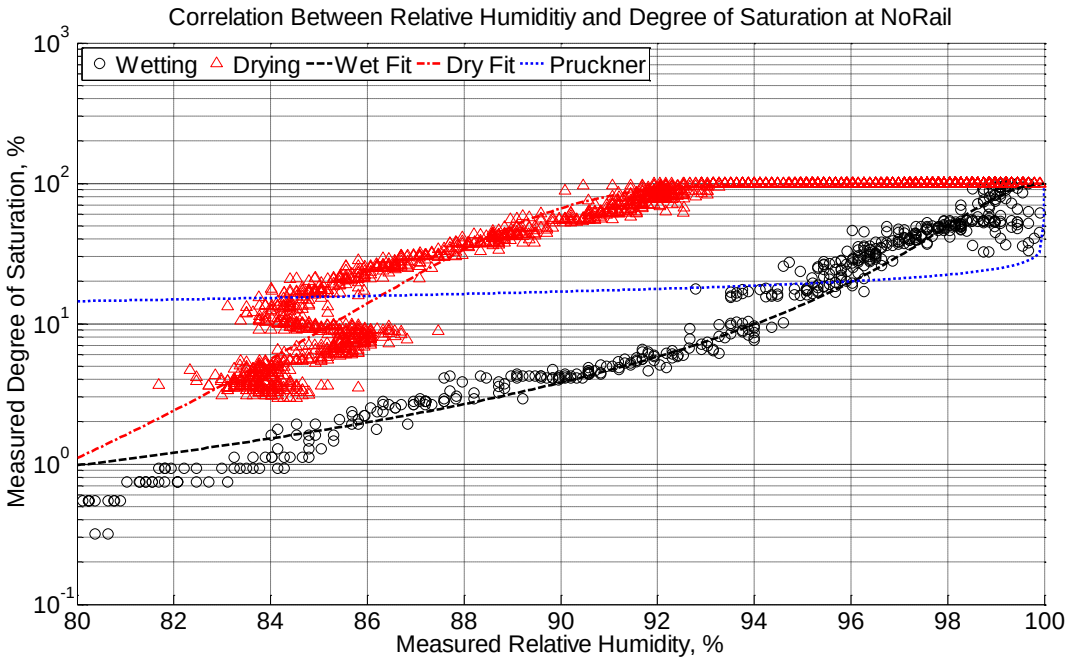

Figure 3-19 Correlation between measured relative humidity and log-scale degree of saturation at depth of 8.5 inches (215.9 mm) from the top surface of a model concrete crosstie (labeled NoRail) without a polyurethane pad nor rail installed in model ballast in Rantoul, IL. The black circles represent a wetting cycle that occurs from December 6, 2014, though December 13, 2014, while the red triangles represent a drying cycle that occurs from June 20, 2015, through September 11, 2015.

3.6 Summary of Chapter

Concrete crossties are subjected to freeze-thaw climates across North America which can leave them susceptible to freeze-thaw cyclic damage. Model concrete crossties were instrumented with hygrothermal sensors and moisture sensors in order to monitor their internal relative humidity and degree of saturation in model aggregate ballast in Rantoul, IL. A simple adsorption isotherm is applied in order to predict the correlation between degree of saturation and relative humidity. It is found that:

- Relative humidity and degree of saturation steadily increase inside a model concrete crosstie whose cross-sectional dimensions are typical of a conventional concrete crosstie when installed in un-fouled model ballast. Conversely, the two values steadily decrease when dry conditions are maintained.
- Although the persistence of a high relative humidity value, alone, is not sufficient to suggest that the concrete crosstie is saturated, a persistently high degree of saturation

measurement from a moisture sensor is sufficient to make such a claim. The results in this study indicate that model concrete crossties installed in aggregate ballast are often saturated above 86%, meaning that they are susceptible to freeze-thaw damage.

- An adsorption isotherm is not sufficient to characterize the correlation between relative humidity and degree of saturation inside high performance concrete installed in the field. This is likely due to a number of factors, including lack of constant temperature, inability of achieve equilibrium due to fast-changing external environments, and non-constant pore size distribution.
- An empirically fitted set of 3-parameter S-shaped curves can appropriate predict the correlation between relative humidity and degree of saturation of high performance concrete when installed in the field. However, these calibrated curves are subject to modification based on concrete mixture design (affecting the pore size distribution), history of hydration (where a fully hydrated Portland cement paste would have minimal changes in pore structure due to precipitation of solid-phased products), and are path-dependent functions (where intermediary wetting or drying traverse paths that are bounded by the empirically fitted curves). As such, these correlation curves are most useful when appropriately calibrated for a family comparable concrete members.

3.7 References

Adolphs, J., and Setzer, M. J. "Energetic classification of adsorption isotherms." *Journal of Colloid and Interface Science* 184 (1996): 443 – 448.

Beaudoin, J. J., and Cameron, M. "Dimensional changes of hydrated Portland cement paste during slow cooling and warming." *Cement and Concrete Research* 2 (1972): 225 – 240.

Bentz, D. P. "Influence of internal curing using lightweight aggregates on interfacial transition zone percolation and chloride ingress in mortars." *Cement and Concrete Composites* 31 (2009): 285 – 289.

Bentz, D. P., Ehlen, M. A., Ferraris, C. F., and Garboczi, E. J. "Sorptivity-based service life predictions for concrete pavements." *7th International Conference on Concrete Pavements* NIST, Orland, FL (2001): 181 – 193.

Bonnaud, P. A., Ji, Q., Coasne, B., Pellenq, R.J.-M., and van VLiet, K. J. "Thermodynamics of water confined in porous calcium-silicate-hydrates." *Langmuir* 28 (2012): 11422 – 11432.

Carlos, C. "Microscopic observations of internal frost damage and salt scaling." *University of California, Berkeley* (2005): PhD Dissertation.

Collepardi, M. "A state-of-the-art review on delayed ettringite attack on concrete." *Cement and Concrete Composites* 25 (2003): 401 – 407.

Dobruskin, V. K. "Effect of meniscus geometry on equilibrium pressures of the Lennard-Jones liquids." *Langmuir* 24 (2008): 9375 – 9380.

Espinosa, R. M., and Franke, L. "Influence of the age and drying process on pore structure and sorption isotherms of hardened cement paste." *Cement and Concrete Research* 36 (2006): 1969 – 1984.

Fagerlund, G. "The critical degree of saturation method of assessing the freeze/thaw resistance of concrete." *RILEM Committee 4* (1977).

Ferraris, C. F. "Alkali-Silica Reaction and High Performance Concrete." NISTIR 5742, Building and Fire Research Laboratory (1995). Report.

Hansen, K. K. "Sorption Isotherms – A Catalogue." *Technical Report* 162 (1986). The Technical University of Denmark. Department of Civil Engineering. Building Materials Laboratory.

Henkensiefken, R., Castro, J., Bentz, D., Nantung, T., and Weiss, J. "Water absorption in internally cured mortar made with water-filled lightweight aggregate." *Cement and Concrete Research* 39 (2009): 883 – 892.

Kovler, K. "Setting and hardening of gypsum-Portland cement-silica fume blends, Part I: Temperature and setting expansion." *Cement and Concrete Research* 28 (1998): 423 – 437.

Li, W., Pour-Ghaz, M., Castro, J., and Weiss, J. "Water absorption and critical degree of satuation relating to freeze-thaw damage in concrete pavement joints." *Journal of Materials in Civil Engineering* 24 (2012): 299 – 307.

Litvan, G. G. (1988). "The mechanism of frost action in concrete-theory and practical implications." *Proceedings of Workshop on Low Temperature Effects on Concrete*, National Research Council of Canada, Montreal, Canada, 115 – 134.

Litvan, G. G., and Sereda, P. J. (1980). "Freeze-thaw durability of porous building materials." *Durability of Building Materials and Components*, ASTM STP 691, P. J. Sereda and G. G. Litvan, Eds. ASTM International, West Conshohocken, PA, 455 – 463.

Maxim Integrated. (March 2013). *DS1923 Revision 5*. Retrieved from http://datasheets.maximintegrated.com/en/ds/DS1923.pdf.

Mindess, S., Young, J. F., and Darwin, D. *Concrete 2nd Edition*. 2003, Upper Saddle River, NJ: Prentice Hall.

Poyet, S., and Charles, S. "Temperature dependence of the sorption isotherms of cement-based materials: Heat of sorption and Clausius-Clapeyron formula." *Cement and Concrete Research* 39 (2009): 1060 – 1067.

Pruckner, F. "Relative humidity measurements for assessing moisture conditions in concrete structures." *Beton-und Stahlbetonbau* 108 (2013): 865 – 874. Language: German.

Rotronic Instrument Corp. (December 2005). *The Rotronic Humidity Handbook*. Retrieved from http://www.southeastern-automation.com/PDF/Rotronic/Humidity_Handbook.pdf.

Shimada, H., Sakai, K., and Litvan, G. G. (1991). "Acoustic emissions of mortar subjected to freezing and thawing." *Durability of Concrete: Second International Conference* V. M. Malotra, Ed. American Concrete Institute, Detroit, MI, 263 – 278.

Swamy, R. N. (Ed). *The Alkali-Silica Reaction in Concrete*. 2002, New York: CRC Press.

Tesárek, P., Černý, R., Drchalová, J., and Rovnaníková, P. "Mechanical, hygric and thermal properties of flue gas desulfurization gypsum." *Acta Polytechnica* 44 (2004): 83 – 88.

Xi, Y., Bažant, Z. P., and Jennings, H. M. "Moisture diffusion in cementitious materials." *Advanced Cement Based Materials* 1 (1994): 248 – 257.

Yang, Q. "Inner relative humidity and degree of saturation in high-performance concrete stored in water or salt solution for 2 years." *Cement and Concrete Research* 29 (1999): 45 – 43.

Zeman, J. C., Edwards, J. R., Lange, D. A., and Barkan, C. P. L. "Evaluating the potential for damaging hydraulic pressure in the concrete tie rail seat." *Proceedings of the 2010 Joint Rail Conference* (2010): Urbana, IL.